


SATELLITE SPECTRA OF HELIUMLIKE NICKEL

By

H. Hsuan et al.

FEBRUARY 1987

PLASMA
PHYSICS
LABORATORY 

H. Hsuan, M. Bitter, K. W. Hill, S. von Goeler,
B. Grek, D. Johnson, L. C. Johnson, and S. Sesnic
Plasma Physics Laboratory, Princeton University,

P.O. Box 451

Princeton, New Jersey 08544

C.P. Bhalla and K.R. Karim

Department of Physics, Kansas State University,

Manhattan, Kansas 66506

F. Bely-Dubau and P. Faucher

Observatoire de Nice,

BP 139, F-06003 Nice Cedex, France

DISCLAIMER

This report was prepared as an account of work sponsored by an agency of the United States Government. Neither the United States Government nor any agency thereof, nor any of their employees, makes any warranty, express or implied, or assumes any legal liability or responsibility for the accuracy, completeness, or usefulness of any information, apparatus, product, or process disclosed, or represents that its use would not infringe privately owned rights. Reference herein to any specific commercial product, process, or service by trade name, trademark, manufacturer, or otherwise does not necessarily constitute or imply its endorsement, recommendation, or favoring by the United States Government or any agency thereof. The views and opinions of authors expressed herein do not necessarily state or reflect those of the United States Government or any agency thereof.

ABSTRACT

Spectra of heliumlike nickel, NiXXVII, have been observed from Tokamak Fusion Test Reactor (TFTR) plasmas with a high resolution crystal spectrometer. The experimental arrangement permits simultaneous observation of the heliumlike resonance line, the intercombination and forbidden lines, and all the associated satellites due to transitions $1s^2n\ell - 1s2\ell'n\ell'$ with $n \geq 2$. Relative wavelengths and line intensities can thus be determined very accurately. The observed spectral data are in good agreement with results from the present Hartree-Fock-Slater atomic model calculations and predictions from the Z-expansion method.

MASTER

I. INTRODUCTION

Heliumlike and hydrogenlike spectra of high- Z ions are of interest for the diagnostics of tokamak plasmas and solar flares, and they are also important for the testing of atomic theories which must include relativistic and quantum electrodynamical effects.¹⁻³ So far, spectra of heliumlike and hydrogenlike ions with $Z \leq 26$, especially Ar, Ti, Cr, and Fe, have been studied in detail from tokamak plasmas.⁴⁻¹² With the new generation of tokamaks, e.g., the Joint European Torus (JET)¹³ and the Tokamak Fusion Test Reactor (TFTR),¹⁴ which are designed to obtain fusion breakeven, it is possible to maintain plasmas of large volumes ($V > 40 \text{ m}^3$) with electron densities, n_e , in the range from 10^{19} to 10^{20} m^{-3} and electron temperatures $T_e > 5 \text{ keV}$ in steady-state conditions for several seconds. Under these conditions, elements with $Z > 26$ can be observed in the heliumlike and hydrogenlike charge states.

In this paper spectra of heliumlike nickel, NiXXVII, are presented as well as a detailed comparison of the experimental data with results from Hartree-Fock-Slater atomic model calculations,^{15,16} and the results obtained by the Z -expansion method.¹⁷⁻¹⁹ The experimental results are presented in Sec. II. The identification of the observed spectral features and comparison of wavelengths and intensities with theoretical predictions are described in Sec. III. The analysis results and diagnostic applications are discussed in Sec. IV.

II. EXPERIMENT

The measurements have been performed on TFTR with a new crystal spectrometer which consists of three crystals and position-sensitive detectors in the Johann configuration.²⁰ The instrument has been designed to record

spectra from three approximately vertical chords of the plasma minor section in order to measure radial profiles of the ion temperature and plasma rotation velocity from the Doppler broadening and Doppler shift of X-ray lines from metal impurity ions of Ti, Cr, Fe, and Ni. Traces ($\lesssim 0.1\%$) of these elements are present in TFTR plasmas from the Inconel ($\sim 70\%$ Ni, $\sim 15\%$ Cr, $\sim 7\%$ Fe, $\sim 2.5\%$ Ti) bellow protective plates and the stainless steel vacuum vessel. The resolution of the spectrometer is $\lambda/\Delta\lambda > 10,000$. 128 spectra per crystal are recorded during a TFTR discharge for time-resolved measurements of these plasma parameters.²¹ The wavelength range obtained with a single spectrometer setting covers the entire spectral range of the dielectronic satellite lines of heliumlike ions. It is thus possible to determine the satellite to resonance line intensity ratios accurately from a simultaneous measurement of these lines. This is important for diagnostic applications of these intensity ratios for measurements of the electron temperature, the ionization equilibrium, and ion transport.⁹⁻¹²

The nickel spectra were obtained from a central vertical chord (at a major radius $R = 249$ cm) with a 2243 quartz crystal ($2d = 2.028$ Å) of the size of 1.5 in. \times 6 in. \times 0.030 in. The curvature radius was $R_c = 1013$ cm, and the spectral resolution was $\lambda/\Delta\lambda = 18,000$. Figure 1 shows a measured spectrum of NiXXVII. The data were obtained from the steady-state phase of a TFTR discharge with a central electron temperature of 4 keV and a very low central electron density, $n_e(0) = 8 \times 10^{12}$ cm⁻³. The radial profiles of the electron temperature and electron density as measured by laser Thomson scattering are shown in Fig. 2. Under these conditions the plasma electrons and plasma ions are weakly coupled, such that the ion temperature is well below the electron temperature. The spectral features are, therefore, well resolved and not obscured by Doppler broadening. Moreover, the collisionally excited

lithiumlike and berylliumlike satellites are expected to be prominent spectral features, since substantial deviations from coronal equilibrium occur under these experimental conditions.²²

III. LINE IDENTIFICATION

The nine prominent features of the spectrum shown in Fig.1 have been identified as the resonance line, the intercombination lines, and the forbidden line of heliumlike nickel, NiXXVII, and the associated strong lithiumlike and berylliumlike satellites of the resonance line. The transitions of these spectral features are listed in Table 1. The key letters correspond to Gabriel's notation.²³ Also listed in Table 1 are the theoretical wavelengths and line strengths, $F_2(sf)$, for the strong dielectronic satellites as obtained by Vainshtein and Safronova^{17,18} and from our present calculations which are described below. The channel numbers, N , in column 4 of Table 1 correspond to the center positions of the observed spectral features. They were obtained from a least-mean-squares fit of Voigt functions, and they were then used for determination of the experimental wavelengths using the following relation:

$$\lambda = 2d \sin (\theta_0 + \Delta\theta) \quad , \quad (1)$$

where $\Delta\theta$ (degree) = $3.719 \times 10^{-3}(N - N_0)$ corresponds to the dispersion of the instrument. N_0 is the center channel number of peak 1. Since the spectrometer is not absolutely calibrated, the experimental wavelengths are given in reference to the theoretical wavelength values for the resonance line w by assigning $\lambda_w^{\text{theor.}} = 2d \sin \theta_0$ to the center channel N_0 of peak 1. We note from Table 1 that both sets of theoretical wavelengths are in good

agreement with the experimental values. For a more detailed comparison between theory and experiment synthetic spectra were constructed from the theoretical transition arrays in Table 1 as well as from the transition arrays for the $n = 3, 4$ lithiumlike satellites, which are given in Table 2 and in Ref. 19. To facilitate a direct comparison with the experimental data, channel numbers were converted into wavelengths by using Eq. (1), and Voigt functions were then calculated from the theoretical transitions for this wavelength array. The synthetic spectra are shown in Figs. 3 and 4 together with the experimental data. The calculated contributions from the different spectral components, i. e., the heliumlike lines, the dielectronic lithiumlike satellites, and the collisionally excited lithiumlike and berylliumlike satellites, to the total synthetic spectrum are shown separately by the shaded areas in subfigures (b), (c), and (d). The line intensities of the synthetic spectrum were normalized to the intensity of the resonance line w . The intensities of the heliumlike lines x , y , and z were obtained from the following expression:

$$\frac{I_{x,y,z}}{I_w} = \frac{C_{x,y,z}(T_e)}{C_w(T_e)} \quad (2)$$

Values for the excitation rate coefficients, $C_{x,y,z,w}$, were calculated using the methods described in Refs. 7 and 9. Here, we included only the contributions from direct excitation, radiative cascade transitions, and collisional resonances, but we neglected the contribution to the line z from the inner-shell ionization. The relative intensities for the dielectronic satellites were calculated from the following expression:

$$\frac{I_s^{\text{diel.}}}{I_w} = \frac{1}{2C_w(T_e)} \left[\frac{(2\pi\hbar^2)}{\pi_e kT_e} \right]^{3/2} F_2(\text{sf}) \exp\left(\frac{-E_s}{kT_e}\right) \quad (3)$$

with

$$F_2(sf) = \frac{g_s A_a(s)A_r(sf)}{A_T(s)}$$

$F_2(sf)$ is the satellite line strength; E_s is the Auger electron energy; $A_T(s)$ is the total transition rate of the autoionizing state $|s\rangle$; $A_a(s)$ and $A_r(sf)$ are, respectively, the Auger transition rate to the ground state and the radiative rate of $|s\rangle$ to the final state $|f\rangle$.

In the present calculations, the Hartree-Fock-Slater atomic model (HFS) was employed to obtain the single-particle wave functions. These wave functions were then used to calculate the radial Auger and electric dipole matrix elements. Configuration state functions belonging to the same complex were allowed to mix. The diagonal elements of the energy matrix were corrected for relativistic effects. The effects due to spin-orbit interaction were included. The energy matrices were diagonalized to obtain correlated atomic state functions and energies; these were used in calculating transition rates. For the w, x, y, j, q, β , and z lines the wavelengths were calculated using the multi-configuration Dirac-Fock model including radiative corrections of quantum electrodynamics. The difference between the Dirac-Fock wavelength and the Hartree-Fock-Slater wavelength for the j-line was 0.0025 Å. This was added to the wavelengths of all other dielectronic satellite lines. The synthetic spectrum shown in Fig. 3 was constructed from the HFS results. In Ref. 17, the Z-expansion method is used to calculate the atomic quantities which were used in the synthetic spectrum shown in Fig. 4.

The intensity of the collisionally excited lithiumlike (berylliumlike) satellites was obtained from the following expression:

$$\frac{I_s^{\text{coll.}}}{I_w} = \frac{C_s(T_e)}{C_w(T_e)} \frac{n_{\text{Ni}^*}}{n_{\text{NiXXVII}}} \quad (4)$$

where n_{Ni^*} ($= n_{\text{NiXXVI}}$ or n_{NiXXV}) and n_{NiXXVII} are the densities of lithiumlike or (berylliumlike) and heliumlike nickel. $C_s(T_e)$ is the rate coefficient for electron impact excitation of the lithiumlike (or berylliumlike) ion from the ground state.

The synthetic spectra were calculated for the experimentally observed electron and ion temperatures of $T_e = 4$ keV and $T_i = 2$ keV, respectively. Values of $n_{\text{NiXXVI}}/n_{\text{NiXXVII}} = 0.75$ and $n_{\text{NiXXV}}/n_{\text{NiXXVII}} = 0.1$ for the relative abundance of heliumlike, lithiumlike, and berylliumlike nickel were chosen to obtain a best fit with the observed spectrum.

IV. DISCUSSION

The detailed comparisons shown in Figs. 3 and 4 indicate that the predictions from both theories are in very good agreement with the experiment. The predictions differ only slightly with respect to the wavelength for the satellite r (feature 6), where the value of Vainshtein and Safronova is in somewhat better agreement with the experiment than the value obtained from the present calculations. The predicted intensities for feature 3 are in both cases slightly higher than the observed value.

The observed NiXXVII spectra confirm the trend of the charge-dependent wavelength shifts reported in Ref. 24. In particular, we observe that the satellite q overlaps with the y line. Similarly, the satellite β is very close to the line z. On the other hand, the dielectronic satellite k and the collisionally excited satellite r are well separated. These charge-dependent wavelength shifts imply that the line q is no longer appropriate for the diagnostic of the relative abundance of the lithiumlike and heliumlike charge states. The satellite r can be used instead.

The values for the abundance of NiXXV and NiXXVI relative to that of NiXXVII, which were obtained from the analysis in Sec. III, are substantially larger than the predictions²⁵ for the fractional abundance of these charge states in coronal equilibrium (see Fig. 5). Modeling calculations, such as those described in Ref. 9, make it possible to deduce values for the radial ion transport coefficients from these observed deviations. The resonance lines w of NiXXVII as well as FeXXV have been successfully used for Doppler measurements. Doppler ion temperatures $T_i > 20$ keV have recently been measured in TFTR experiments with intense neutral beam heating from these impurity lines.^{26,27}

ACKNOWLEDGMENTS

The technical assistance of J. Gorman, J. Lehner, P. Howard, and the TFTR operating crew is highly appreciated. We also gratefully acknowledge the continuing support of Dr. K.M. Young, Dr. H.P. Furth, Dr. R. Goldston, Dr. D. Grove, Dr. D. M. Meade, and Dr. P. H. Rutherford.

This work was supported by U.S. Department of Energy Contract No. DE-AC02-76-CHO-3073. Two of us (G.P.B. and K.R.K.) were supported by the Division of Chemical Sciences, Office of Basic Energy Sciences, Office of Energy Research, and the U.S. Department of Energy. Computations of excitation rate coefficients were carried out on the NAS 980 - CIRCE computer in Orsay, France.

REFERENCES

- ¹J. Dubau and S. Volonte, Rep. Prog. Phys. 43, 199 (1980).
- ²C. De Michelis and M. Mattioli, Nucl. Fusion 21, 677 (1981).
- ³R. K. Janev, L. P. Presnyakov, and V.P. Shevelko, in Physics of Highly Charged Ions, Vol. 13 of Springer Series in Electrophysics, edited by G. Ecker (Springer, Berlin, 1985).
- ⁴TFR Group and F. Bombarda, in Proceedings of the 11th European Conference on Controlled Fusion and Plasma Physics, Aachen, FRG, 1983, edited by S. Methfessel (European Physical Society, Aachen, 1983), Vol. 7D, Part I, p. 89.
- ⁵TFR Group, F. Bombarda, F. Bely-Dubau, P. Faucher, M. Cornille, J. Dubau, and M. Loulergue, Phys. Rev. A 32, 2374 (1985).
- ⁶E. Kallne, J. Kallne, A. Dalgarno, E. S. Marmor, J. E. Rice, and A. K. Pradhan, Phys. Rev. Lett. 52, 2245 (1984).
- ⁷F. Bely-Dubau, P. Faucher, L. Steenman-Clark, M. Bitter, S. von Goeler, K. W. Hill, C. Camhy-Val, and J. Dubau, Phys. Rev. A 26, 3459 (1982).
- ⁸P. Lee, A. J. Lieber, and S. S. Wojtowicz, Phys. Rev. A 31, 3996 (1985).
- ⁹M. Bitter, K. W. Hill, M. Zarnstorff, S. von Goeler, R. Hulse, L. C. Johnson, N. R. Sauthoff, S. Sesnic, K. M. Young, M. Tavernier, F. Bely-Dubau, P. Faucher, M. Cornille, and J. Dubau, Phys. Rev. A 32, 3011 (1985).
- ¹⁰TFR Group, J. Dubau, and M. Loulergue, J. Phys. B 15, 1007 (1981).
- ¹¹M. L. Apicella, R. Bartiromo, F. Bombarda, and R. Giannella, Phys. Lett. 98A, 174 (1983).

- ¹²M. Bitter, K. W. Hill, N. R. Sauthoff, P. C. Efthimion, E. Meservey, W. Roney, S. von Goeler, R. Horton, and W. Stodiek, *Phys. Rev. Lett.* 43, 129 (1979).
- ¹³R. J. Bickerton, *Plasma Phys. Controlled Fusion*, 26, 1055 (1984).
- ¹⁴K. M. Young et al., *Plasma Phys. Controlled Fusion*, 26, 11 (1984).
- ¹⁵C.P. Bhalla and K.R. Karim, *Phys. Rev. A* 34, 3525 (1986).
- ¹⁶K.R. Karim and C.P. Bhalla, to be published in *Phys. Rev. A*.
- ¹⁷L. A. Vainshtein and U. I. Safronova, *At. Data Nucl. Data Tables* 21, 49 (1978).
- ¹⁸U. I. Safronova, A. M. Urnov, and L. A. Vainshtein, *Proc. P. N. Lebedev. Phys. Inst. [Acad. Sci. USSR]* 119, 13 (1980).
- ¹⁹L. A. Vainshtein and U. I. Safronova, *At. Data Nucl. Data Tables* 25, 311 (1980).
- ²⁰H. Johann, *Z. Phys.* 69, 189 (1931).
- ²¹M. Bitter, K. W. Hill, S. Cohen, S. von Goeler, H. Hsuan, L.C. Johnson, R. Raftopoulos, M. Reale, N. Schechtman, S. Senic, F. Spinos, J. Timberlake, S. Weicher, N. Young, and K. M. Young, *Rev. Sci. Instrum.* 57, 2145 (1986).
- ²²M. Bitter, S. von Goeler, N. Sauthoff, K. W. Hill, K. Brau, D. Eames, M. Goldman, E. Silver and W. Stodiek, in *Inner-Shell and X-Ray Physics of Atoms and Solids*, edited by D. J. Fabian, H. Kleinpoppen, and I. M. Watson (Plenum Press, New York, 1981), p.861.
- ²³A. H. Gabriel, *Mon. Not. R. Astron. Soc.* 160, 99 (1972).
- ²⁴TFR Group, M. Cornille, J. Dubau, and M. Loulergue, *Phys. Rev. A* 32, 3000 (1985).
- ²⁵C. Breton, C. De Michelis, M. Finkenthal, and M. Matioli, Fontenay-aux-Roses Laboratory Report No. EUR-CEA-FC-948, 1978 (unpublished).

²⁶H. Hsuan, M. Bitter, S. von Goeler, S. Sesnic, J. Timberlake, and S. Cohen,
Bull. Am. Phys. Soc. 31, 1611 (1986).

²⁷M. Bitter, K. W. Hill, S. Hiroe, H. Hsuan, S. von Goeler, S. Sesnic, and
M. Zarnstorff, Bull. Am. Phys. Soc. 31, 1414 (1986).

TABLE CAPTIONS

Table 1. Experimental wavelengths and theoretical predictions for the resonance, intercombination, and forbidden lines of NiXXVII, and the associated satellite lines due to transitions $1s^2 2l - 1s 2l' 2l''$. Wavelengths are in Å and satellite line strengths $F_2(sf)$ are in units of $10^{13} s^{-1}$.

Table 2. Atomic data calculated with the HFS atomic model for satellite line transitions: $1s^2 n l - 1s 2l' n l''$ with $n = 3, 4$ of NiXXVI. The wavelengths are in Å. The line strengths $F_2(sf)$ are in units of $10^{13} s^{-1}$. Lines with F_2 - values less than $10^{13} s^{-1}$ are not listed.

Peak	key	Transition	N	$\lambda_{\text{expt.}}$	$\lambda_{\text{theor.}}^{(a)}$	$F_2^{(a)}(\text{sf})$	$\lambda_{\text{expt.}}$	$\lambda_{\text{theor.}}^{(b)}$	$F_2^{(b)}(\text{sf})$
1	w	$1s^2 1S_0 - 1s 2p 1P_1$	146.11	1.5879 ^a	1.5879		1.5886 ^a	1.5886	
2	x	$1s^2 1S_0 - 1s 2p 3P_2$	193.18	1.5917	1.5918		1.5924	1.5925	
3	a	$1s^2 2s 2S_{1/2} - 1s 2s 2p 2P_{3/2}$	210.21	1.5931	1.5926	0.0106	1.5938	1.5935	2.40
	b	$1s^2 2p 2P_{1/2} - 1s 2p^2 2P_{3/2}$			1.5929	0.157			
	m	$1s^2 2p 2P_{3/2} - 1s 2p^2 2S_{1/2}$			1.5931	6.00		1.5940	4.98
	t	$1s^2 2s 2S_{1/2} - 1s 2s 2p 2P_{1/2}$			1.5934	12.8		1.5940	11.12
4	y	$1s^2 1S_0 - 1s 2p 3P_1$	248.04	1.5962	1.5959		1.5969	1.5968	
	q	$1s^2 2s 2S_{1/2} - 1s 2s 2p 2P_{3/2}$			1.5965	0.412		1.5972	
5	a	$1s^2 2p 2P_{3/2} - 1s 2p^2 2P_{3/2}$	267.17	1.5978	1.5973	17.5	1.5985	1.5981	14.40
	k	$1s^2 2p 2P_{1/2} - 1s 2p^2 2D_{3/2}$			1.5980	38.1		1.5987	39.32
	d	$1s^2 2p 2P_{1/2} - 1s 2p^2 2P_{1/2}$			1.5980	0.166			
6	r	$1s^2 2s 2S_{1/2} - 1s 2s 2p 2P_{1/2}$	283.50	1.5991	1.5992	6.93	1.5998	1.6003	7.19
7	J	$1s^2 2p 2P_{3/2} - 1s 2p^2 2D_{5/2}$	298.31	1.6003	1.6005	58.0	1.6010	1.6011	53.49
8	L	$1s^2 2p 2P_{3/2} - 1s 2p^2 2D_{3/2}$	330.47	1.6029	1.6024	5.73	1.6036	1.6033	4.84
	z	$1s^2 1S_0 - 1s 2s 3S_1$			1.6031			1.6035	
9	B	$1s^2 2s^2 1S_0 - 1s 2s^2 2p 1P_1$	340.32	1.6037			1.6044	1.6047	

^aThe experimental wavelengths are normalized to the theoretical values for the $1s^2 1S_0 - 1s 2p 1P_1$ transition.

^aReference 17, 18

^bPresent HFS Calculations

Table 1

Final State $ f\rangle$	Autoionizing State $ s\rangle$	λ (Å)	$F_2(sf)$ ($\times 10^{13} s^{-1}$)
$1s^2 3p 2P_{3/2}$	$1s 2p(^1P)3p 2S_{1/2}$	1.5892	2.66
$1s^2 4p 2P_{3/2}$	$1s 2p(^1P)4p 2P_{3/2}$	1.5897	1.93
$1s^2 4p 2P_{1/2}$	$1s 2p(^1P)4p 2D_{3/2}$	1.5898	4.82
$1s^2 4p 2P_{3/2}$	$1s 2p(^1P)4p 2D_{5/2}$	1.5899	3.94
$1s^2 3p 2P_{3/2}$	$1s 2p(^1P)3p 2P_{3/2}$	1.5903	6.24
$1s^2 3s 2S_{1/2}$	$1s 2p(^1P)3s 2P_{1/2}$	1.5904	1.26
$1s^2 3p 2P_{1/2}$	$1s 2p(^1P)3p 2D_{3/2}$	1.5906	12.82
$1s^2 3p 2P_{3/2}$	$1s 2p(^1P)3p 2D_{5/2}$	1.5912	15.94
$1s^2 4d 2D_{5/2}$	$1s 2p(^1P)4d 2F_{5/2}$	1.5919	1.97
$1s^2 4d 2D_{3/2}$	$1s 2p(^1P)4d 2D_{5/2}$	1.5920	1.07
$1s^2 4d 2D_{5/2}$	$1s 2p(^1P)4d 2F_{7/2}$	1.5922	5.05
$1s^2 3p 2P_{3/2}$	$1s 2p(^3P)3p 2D_{5/2}$	1.5936	1.86
$1s^2 3d 2D_{3/2}$	$1s 2p(^1P)3d 2F_{5/2}$	1.5951	3.36
$1s^2 3d 2D_{5/2}$	$1s 2p(^1P)3d 2F_{5/2}$	1.5956	3.09
$1s^2 3d 2D_{5/2}$	$1s 2p(^1P)3d 2F_{7/2}$	1.5963	9.98
$1s^2 3s 2S_{1/2}$	$1s 2p(^3P)3s 2P_{1/2}$	1.5966	5.09
$1s^2 4p 2P_{3/2}$	$1s 2p(^3P)4p 2D_{3/2}$	1.5975	1.03
$1s^2 4p 2P_{3/2}$	$1s 2p 4p 4D_{5/2}$	1.5980	1.67
$1s^2 3p 2P_{3/2}$	$1s 2p 3p 4D_{5/2}$	1.5997	2.33
$1s^2 4s 2S_{1/2}$	$1s 2p(^3P)4s 2P_{1/2}$	1.6032	1.01
$1s^2 3p 2P_{3/2}$	$1s 3s(^3S)2s 2S_{1/2}$	1.6050	1.41

Table 2

FIGURE CAPTIONS

- FIG. 1. Satellite spectrum of NiXXVII. The data were recorded from an ohmically heated TFTR discharge during its steady-state phase.
- FIG. 2. Radial profiles of the electron temperature and the electron density as measured by the TFTR Thomson scattering diagnostic.
- FIG. 3. Comparison of the observed NiXXVII spectrum with a synthetic spectrum constructed from the results obtained by the present HFS atomic model calculations. The experimental data are shown in (a). The contributions from the heliumlike lines, the dielectronic lithiumlike satellites, and the collisionally excited lithiumlike and beryllium-like satellites to the synthetic spectrum are shown by the shaded areas in (b), (c), and (d), respectively. The envelope shown in (b), (c), and (d) is the total synthetic spectrum, i.e., the sum of the various components.
- FIG. 4. Comparison of the observed NiXXVII spectrum with a synthetic spectrum calculated from the theory of Vainshtein and Safronova.¹⁵⁻¹⁷ The experimental data are shown in (a). The contributions from the helium-like lines, the dielectronic lithiumlike satellites, and the collisionally excited lithiumlike and berylliumlike satellites to the synthetic spectrum are shown by the shaded areas in (b), (c), and (d), respectively. Also shown in (b), (c), and (d) is the total synthetic spectrum, i.e., the sum of the various components.
- FIG. 5. Fractional abundance of the ionization states of nickel for coronal equilibrium.²⁶

86X1469

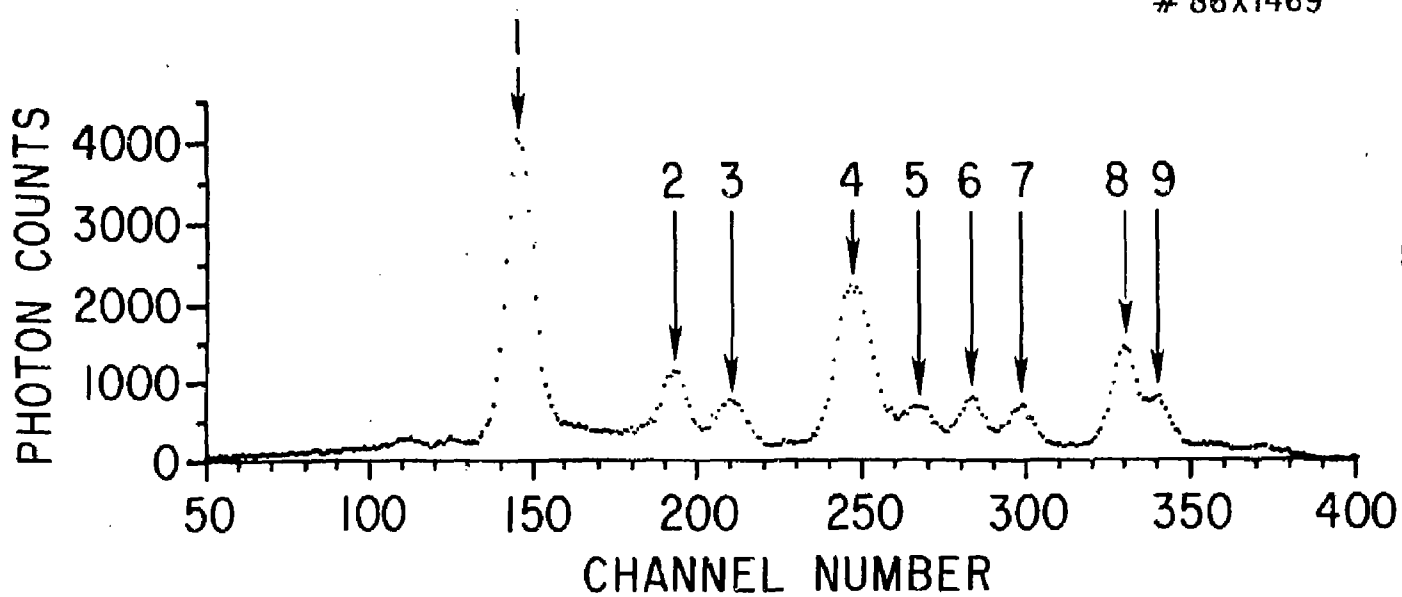


Fig. 1

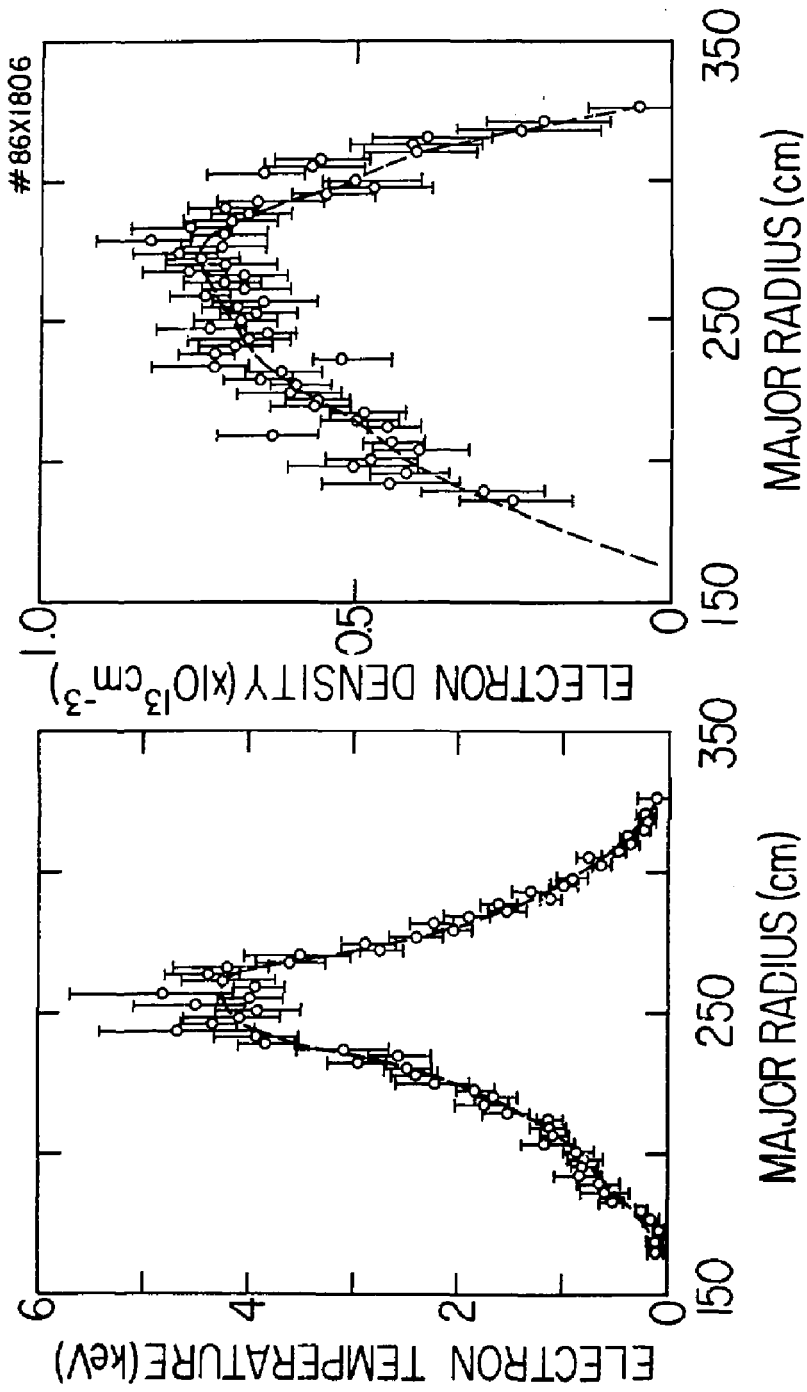


FIG. 2

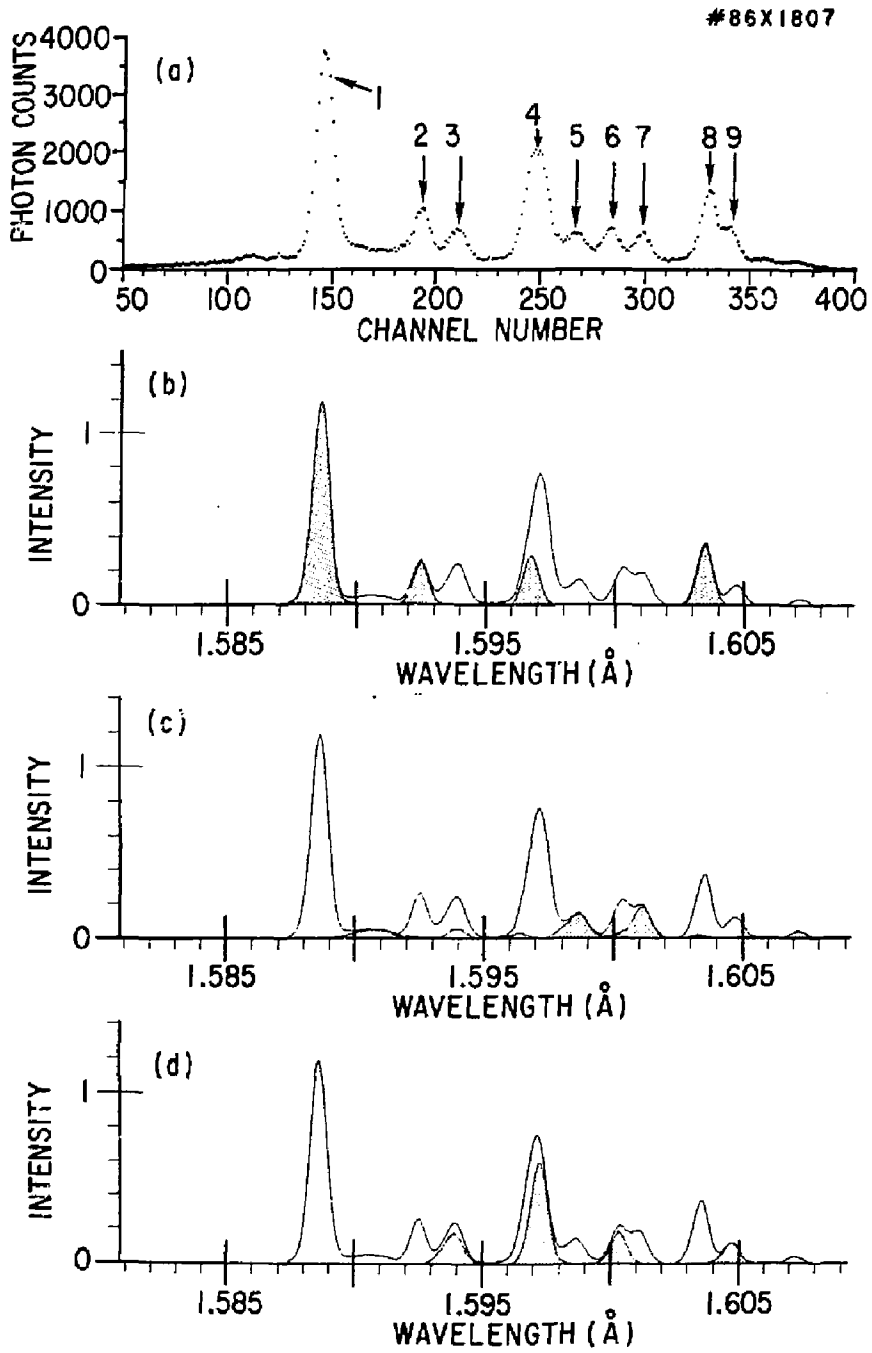


Fig. 3

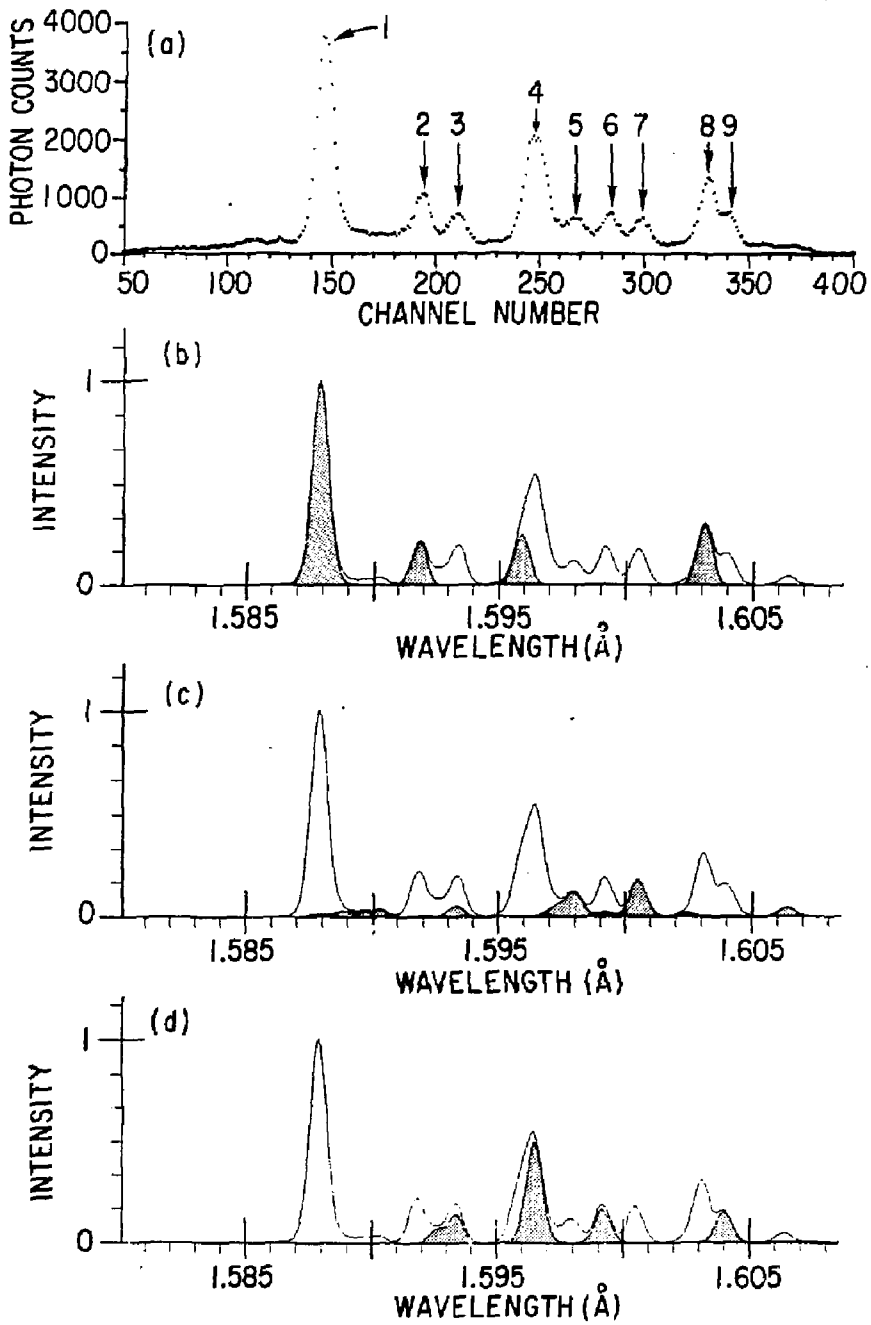


Fig. 4

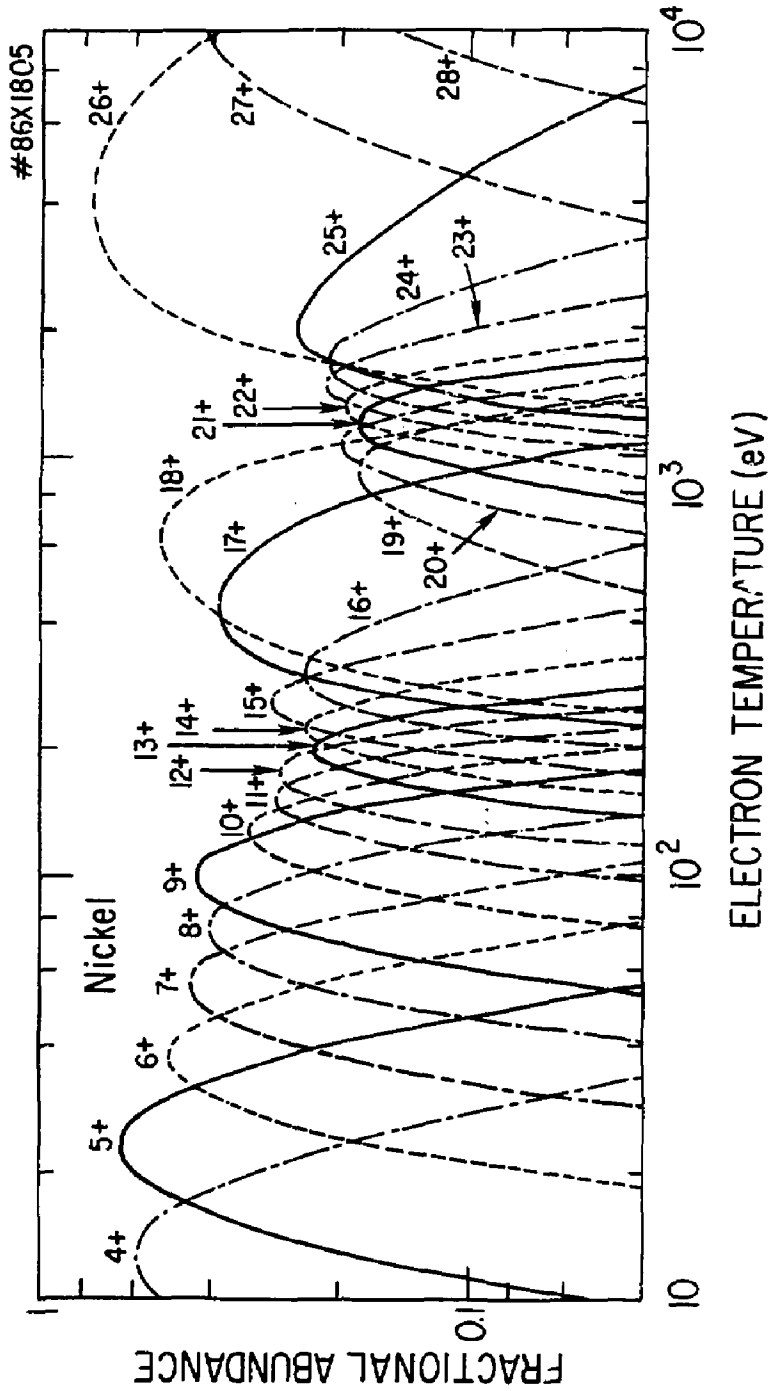


Fig. 5

EXTERNAL DISTRIBUTION IN ADDITION TO UC-20

Dr. Frank J. Paoloni, Univ of Wollongong, AUSTRALIA
Prof. M.H. Brennan, Univ Sydney, AUSTRALIA
Plasma Research Lab., Australian Nat. Univ., AUSTRALIA
Prof. I.R. Jones, Flinders Univ., AUSTRALIA
Prof. F. Cap, Inst Theo Phys., AUSTRIA
Prof. M. Heindler, Institut für Theoretische Physik, AUSTRIA
M. Goossens, Astronomisch Instituut, BELGIUM
Ecole Royale Militaire, Lab de Phys Plasmas, BELGIUM
Com. of European, Dg XII Fusion Prog, BELGIUM
Prof. R. Boucique, Laboratorium voor Natuurkunde, BELGIUM
Dr. P.H. Sakanaka, Univ Estadual, BRAZIL
Instituto De Pesquisas Espaciais-INPE, BRAZIL
Library, Atomic Energy of Canada Limited, CANADA
Dr. M.P. Bachynski, MPB Technologies, Inc., CANADA
Dr. H.M. Skarsgard, Univ of Saskatchewan, CANADA
Dr. H. Barnard, University of British Columbia, CANADA
Prof. J. Teichmann, Univ. of Montreal, CANADA
Prof. S.R. Greenivasan, University of Calgary, CANADA
Prof. Tudor W. Johnston, INRS-Energie, CANADA
Dr. C.R. James, Univ. of Alberta, CANADA
Dr. Peter Lukac, Komenského Univ, CZECHOSLOVAKIA
The Librarian, Culham Laboratory, ENGLAND
Mrs. S.A. Hutchinson, JET Library, ENGLAND
C. Mouttet, Lab. de Physique des Milieux Ionisés, FRANCE
J. Radet, CEN/CADARACHE - Bat 506, FRANCE
Dr. Tom Mual, Academy Bibliographic, HONG KONG
Preprint Library, Cent Res Inst Phys, HUNGARY
Dr. B. Dasgupta, Saha Inst, INDIA
Dr. R.K. Chhajlani, Vikram Univ. INDIA
Dr. P. Kew, Institute for Plasma Research, INDIA
Dr. Phillip Rosenau, Israel Inst Tech, ISRAEL
Prof. S. Cuperman, Tel Aviv University, ISRAEL
Librarian, Int'l Ctr Theo Phys, ITALY
Prof. G. Rostagni, Univ DI Padova, ITALY
Miss Clelia De Palo, Assoc EURATOM-ENEA, ITALY
Biblioteca, del CNR EURATOM, ITALY
Dr. H. Yamato, Toshiba Res & Dev, JAPAN
Prof. I. Kawakami, Atomic Energy Res. Institute, JAPAN
Prof. Kyoji Nishikawa, Univ of Hiroshima, JAPAN
Direc. Dept. Eg. Tokamak Res. JAERI, JAPAN
Prof. Satoshi Itoh, Kyushu University, JAPAN
Research Info Center, Nagoya University, JAPAN
Prof. S. Tanaka, Kyoto University, JAPAN
Library, Kyoto University, JAPAN
Prof. Nobuyuki Inoue, University of Tokyo, JAPAN
S. Mori, JAERI, JAPAN
M.H. Kim, Korea Advanced Energy Research Institute, KOREA
Prof. D.I. Choi, Adv. Inst Sci & Tech, KOREA
Prof. B.S. Lilley, University of Waikato, NEW ZEALAND
Institute of Plasma Physics, PEOPLE'S REPUBLIC OF CHINA
Librarian, Institute of Phys., PEOPLE'S REPUBLIC OF CHINA
Library, Tsing Hua University, PEOPLE'S REPUBLIC OF CHINA
Z. Li, Southwest Inst. Physics, PEOPLE'S REPUBLIC OF CHINA
Prof. J.A.C. Cabral, Inst Superior Tecn, PORTUGAL
Dr. Octavian Petrus, AL I CUZA University, ROMANIA
Dr. Johan de Villiers, Plasma Physics, AEC, SO AFRICA
Prof. M.A. Heilberg, University of Natal, SO AFRICA
Fusion Div. Library, JEN, SPAIN
Dr. Lennart Stenflo, University of UMEA, SWEDEN
Library, Royal Inst Tech, SWEDEN
Prof. Hans Wilhelmson, Chalmers Univ Tech, SWEDEN
Centre Phys des Plasmas, Ecole Polytech Fed, SWITZERLAND
Bibliotheek, Fom-Inst Voor Plasma-Fysica, THE NETHERLANDS
Dr. D.D. Ryutov, Siberian Acad Sci, USSR
Dr. G.A. Eliseev, Kurchatov Institute, USSR
Dr. V.A. Glukhikh, Inst Electro-Physical, USSR
Dr. V.T. Tolok, Inst. Phys. Tech. USSR
Dr. L.M. Kovrizhnykh, Institute Gen. Physics, USSR
Prof. T.J.M. Boyd, Univ College N Wales, WALES
Nuclear Res. Establishment, Jülich Ltd., W. GERMANY
Bibliothek, Inst. Für Plasmaforschung, W. GERMANY
Dr. K. Schindler, Ruhr Universität, W. GERMANY
ASDEX Reading Rm, IPP/Max-Planck-Institut für
Plasmaphysik, W. GERMANY
Librarian, Max-Planck Institut, W. GERMANY
Prof. R.K. Janev, Inst Phys, YUGOSLAVIA